JOURNAL OF COMPUTATIONAL PHYSICS 56, 513–529 (1984)

A Numerical Study of the Steady Scalar Convective Diffusion Equation for Small Viscosity*

MICHAEL B. GILES

Massachusetts Institute of Technology, Cambridge, Massachusetts 02139

AND

MILTON E. ROSE

Institute for Computer Applications in Science and Engineering, NASA Langley Research Center, Hampton, Virginia 23665

The equation $\nu\nabla^2 u = f_x(u) + g_y(u)$ is studied by means of a compact finite difference scheme and numerical solutions are compared to the analytic inviscid ($\nu = 0$) solutions. The correct internal and external boundary layer behaviour is observed, due to an inherent feature of the scheme which automatically produces upwind differencing in inviscid regions and the correct viscous behaviours in viscous regions.

INTRODUCTION

Consider a domain D with boundary Γ in the xy plane, in which $u(\nu)$ is the solution of the time-independent convection–diffusion equation

$$f_x(u) + g_y(u) = \nu\nabla^2 u \tag{1.1}$$

for $u = \bar{u}$ on Γ. Certain features of this problem can provide useful insights into the Navier–Stokes equations and their inviscid limit, the Euler equations. (We employ terminology suggested by these applications in the following discussion.) In fluid dynamics it is common to obtain the time-independent solutions to these problems by solving the time-dependent problem for large times. In this paper we instead study (1.1) by a time-independent finite difference equation to which rather standard iterative methods will be shown to apply.

A large variety of finite difference methods can be employed to solve this problem in the sense that if $u(\nu, h)$ indicates the solution of a finite difference scheme in which h is a typical mesh length, then $u(\nu, h) \to u(\nu)$ as $h \to 0$ in, say, an L_2 norm. In

* Research was supported by the National Aeronautics and Space Administration under NASA Grant NAG3-9 for the first author and NASA Contracts NAS1-17070 and NAS1-17130 for both authors while they were in residence at ICASE, NASA Langley Research Center, Hampton, VA 23665.

0021-9991/84 $3.00

particular, integrating (1.1) over a subdomain D' with boundary Γ' produces the conservative integral formulation

$$\oint_{\Gamma'} (fn_x + gn_y)\, ds = \oint_{\Gamma'} \nu \nabla u \cdot \mathbf{n}\, ds, \tag{1.2}$$

where $\mathbf{n} = (n_x, n_y)^T$ is the unit normal vector. Conservative finite difference schemes aproximate this equation in each cell. Nonconservative schemes instead approximate the equivalent differential equation

$$au_x + bu_y = \nu \nabla^2 u, \tag{1.3}$$

where $a = \partial f/\partial u$ and $b = \partial g/\partial u$ in each cell. Since $u(\nu)$ is smooth both approaches produce the correct solution in the limit $h \to 0$.

The situation is more complicated for the "inviscid" weak solution u^0 which satisfies

$$\oint_{\Gamma'} (fn_x + gn_y)\, ds = 0, \tag{1.4}$$

for all closed curves Γ'. This is equivalent to the hyperbolic equation

$$au_x^0 + bu_y^0 = 0, \tag{1.5}$$

provided u^0 is differentiable. However, in the inviscid case boundary data may only be prescribed on part of Γ, say Γ^0. Furthermore there may be nonunique solutions with discontinuities (shocks) or closed characteristic curves (recirculating flows) if $a^2 + b^2 = 0$ at points in D.

Many of the essential facts concerning the relationship of the solution $u(\nu)$ of (1.1) with the "physically relevant" solution u^0 of (1.4) are suggested by formal singular perturbation arguments (Kevorkian and Cole [3], Howes [1, 2]). Specifically, in the limit $\nu \to 0$, we expect that the solution $u(\nu)$ of (1.1) converges to the "physical" weak solution u^0 of (1.4) and boundary layers arise on the complement of Γ^0 in Γ, i.e., that part of Γ on which no boundary data is specified for the inviscid problem for u^0.

The use of finite difference schemes to calculate the solution $u(\nu)$ in the limit $\nu \to 0$ introduces a second limiting process $h \to 0$ (Osher [4]). It is natural to consider the different limiting paths by which $u(\nu, h) \to u^0$ as suggested by Fig. 1. The solid arrows indicate limiting processes which are known to be convergent, assuming a consistent stable finite difference scheme. The dotted arrows denote limiting processes which in general may not be convergent, or may converge to a solution different from u^0.

This paper is concerned with investigating a finite difference scheme which offers useful insights into this problem. The scheme has its origin in a compact exponential scheme described by Philips and Rose [5] for time-dependent problems; an application of this scheme to the Navier–Stokes equations was also described by Rose [7]. An effective time-independent solution method is provided by employing

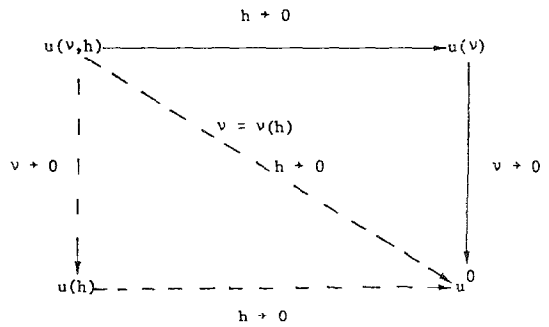

FIG. 1. Typical limiting processes considered in this paper.

the flux-elimination technique described in Phillips and Rose [6]. The first few sections describe the application of these developments to equation (1.1). The relationship of the solution $u(\nu, h)$ to u^0 is then explored by several numerical experiments and simple heuristic analyses.

2. A Compact Scheme

Consider (1.1) in system form

$$\begin{aligned} v_x + w_y &= f_x(u) + g_y(u), \\ v &= \nu u_x, \\ w &= \nu u_y. \end{aligned} \tag{2.1}$$

In a square cell $\pi_{i,j}$, with sides of length $2h$, $u_{i\pm 1/2,j}$, $u_{i,j\pm 1/2}$, $v_{i\pm 1/2,j}$, $w_{i,j\pm 1/2}$ represent the average values of the analytic variables on the corresponding sides of $\pi_{i,j}$ (see Fig. 2).

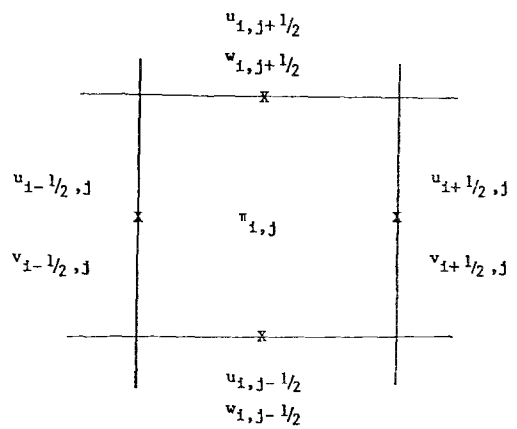

FIG. 2. Location of finite difference variables in a cell $\pi_{i,j}$.

Because solutions of (2.1) are smooth, if h is sufficiently small any solution of (2.1) can be approximated locally by

$$\nu\nabla^2 u = au_x + bu_y,$$

where a, b indicate average values of f_u, g_u in the cell. This equation has elementary solutions $u = \exp(\alpha x + \beta y)$, where $\alpha(a - \nu\alpha) + \beta(b - \nu\beta) = 0$. Any linear combination of four such solutions can be used to obtain a solution having the prescribed average values $u_{i\pm 1/2,j}$, $u_{i,j\pm 1/2}$ on the sides of $\pi_{i,j}$; the corresponding average values $v_{i\pm 1/2,j}$, $w_{i,j\pm 1/2}$ are then related by four algebraic equations. The following algebraic system arises when a solution of the form

$$u = c_1 + c_2 \exp\left(\frac{ax}{\nu}\right) + c_3 \exp\left(\frac{by}{\nu}\right) + c_4 \exp\left(\frac{ax + by}{\nu}\right)$$

is considered:

$$\delta_x v + \delta_y w = \delta_x f + \delta_y g, \tag{2.2a}$$

$$(\mu_x - hp_x\delta_x)\, v = \nu\delta_x u, \tag{2.2b}$$

$$(\mu_y - hp_y\delta_y)\, w = \nu\delta_y u, \tag{2.2c}$$

$$h^2(q_x\delta_x v - q_y\delta_y w) = \nu(\mu_x - \mu_y)\, u, \tag{2.2d}$$

where

$$\delta_x u = (u_{i+1/2,j} - u_{i-1/2,j})/2h,$$

$$\mu_x u = (u_{i+1/2,j} + u_{i-1/2,j})/2,$$

etc., and if $\rho = h/\nu$, $\theta_x = a\rho$, $\theta_y = b\rho$, then

$$p(\theta) = \coth\theta - \theta^{-1}, \qquad p_x \equiv p(\theta_x), \quad p_y \equiv p(\theta_y), \tag{2.3}$$

$$q(\theta) = \theta^{-1}p(\theta), \qquad q_x \equiv q(\theta_x), \quad q_y \equiv q(\theta_y). \tag{2.4}$$

The simple behaviour of $p(\theta)$, $q(\theta)$ is shown in Fig. 3.

The dimensionless parameters θ_x, θ_y are the cell Reynolds numbers which provide a measure of the relative importance of diffusion versus transport effects in a cell. An important feature of this scheme is the manner in which upwind differencing arises when $|\theta| \to \infty$. From (2.3), (2.4),

$$\begin{aligned} p(\theta) &\sim \operatorname{sgn}(\theta) && |\theta| \text{ large}, \\ &\sim \theta/3 && |\theta| \text{ small}; \\ q(\theta) &\sim |\theta|^{-1} && |\theta| \text{ large}, \\ &\sim 1/3 && |\theta| \text{ small}. \end{aligned} \tag{2.5}$$

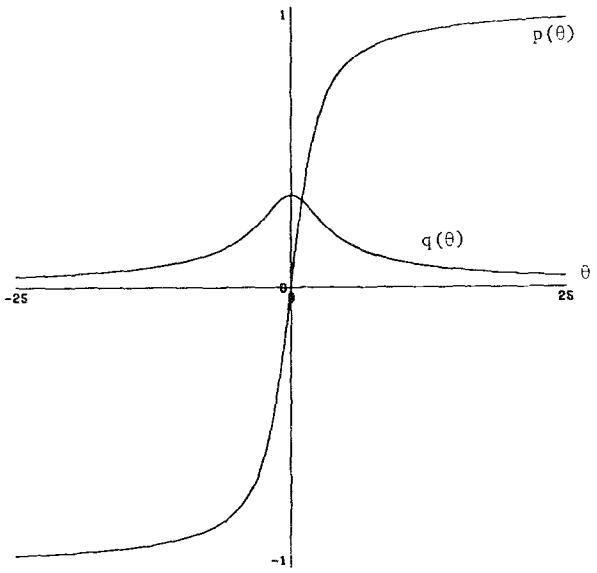

FIG. 3. Graph of $p(\theta)$, $q(\theta)$.

In (2.2b) $(\mu_x - hp_x\delta_x)v$ represents a weighted average of the values $v_{i\pm 1/2,j}$ on the two cell sides. For $|\theta| \to \infty$ the weights tend to 0 or 1, thereby selecting one or another of the values depending on the sign of θ. For $|\theta| \to 0$ the weights tend to $\frac{1}{2}$ giving a simple central average $\mu_x v$.

An important point to note is that Eq. (2.2a) can be interpreted as a finite difference form of the conservative integral Eq. (1.2). Summation over all the cells in domain D yields

$$\sum_{\Gamma} (fn_x + gn_y)\, h = \sum_{\Gamma} (vn_x + wn_y)\, h, \tag{2.6}$$

so the scheme is globally conservative. This is important in ensuring the correct calculation of nonlinear shocks, as will be shown later.

The scheme (2.2) is called compact because it involves only the values of u, v, w associated with an individual cell. Any relationships between values in other cells arise from imposing the further condition that values are continuous across cell boundaries. When a and b are constant in all cells an energy estimate similar to that in [5], [6] can be obtained from (2.2); the result is that the solution $u(v, h)$ converges as $h \to 0$ to a smooth solution $u(v)$ of (2.1) with $O(h^2)$ accuracy.

3. Flux Elimination

Let

$$\begin{aligned} V &= (\mu_x v, \Delta_x v, \mu_y w, \Delta_y w)^{\mathrm{T}}, \\ U &= (\mu_x u, \Delta_x u, \mu_y u, \Delta_y u)^{\mathrm{T}}, \end{aligned} \tag{3.1}$$

where $\Delta = h\delta$. Equations (2.2) may be solved for V to obtain

$$V = R(U), \tag{3.2}$$

where

$$R(U) = \frac{v}{h\sigma} \begin{bmatrix} \sigma \Delta_x u + p_x[(\mu_x - \mu_y)\, u + \rho q_y(\Delta_x f + \Delta_y g)] \\ (\mu_x - \mu_y)\, u + \rho q_y(\Delta_x f + \Delta_y g) \\ \sigma \Delta_y u + p_y[(\mu_y - \mu_x)\, u + \rho q_x(\Delta_x f + \Delta_y g)] \\ (\mu_y - \mu_x)\, u + \rho q_x(\Delta_x f + \Delta_y g) \end{bmatrix} \tag{3.3}$$

in which $\sigma = q_x + q_y$.

Following the method outlined in Phillips and Rose [2] consider two neighboring cells $\pi_{i,j}$ and $\pi_{i+1,j}$ having the common values $u_{i+1/2,j}$ and $v_{i+1/2,j}$ associated with their common side. Clearly

$$v_{i+1/2,j} = (\mu_x + \Delta_x)\, v_{i,j} = (\mu_x - \Delta_x)\, v_{i+1,j}$$

so that

$$(1 \;\; 1 \;\; 0 \;\; 0)\, R_{i,j}(U) = (1 \;\; -1 \;\; 0 \;\; 0)\, R_{i+1,j}(U).$$

Similarly considering the value $w_{i,j+1/2}$ common to cells $\pi_{i,j}$ and $\pi_{i,j+1}$ we also have

$$(0 \;\; 0 \;\; 1 \;\; 1)\, R_{i,j}(U) = (0 \;\; 0 \;\; 1 \;\; -1)\, R_{i,j+1}(U).$$

Using (3.3) there results

$$\begin{aligned} &\mu_x\{\sigma^{-1}[(\mu_x - \mu_y)\, u + \rho q_y(\Delta_x f + \Delta_y g)]\} \\ &\quad - \Delta_x\{\Delta_x u + p_x \sigma^{-1}[(\mu_x - \mu_y)\, u + \rho q_y(\Delta_x f + \Delta_y g)]\} = 0 \qquad (3.4a) \\ &u_y\{\sigma^{-1}[(\mu_y - \mu_x)\, u + \rho q_x(\Delta_x f + \Delta_y g)]\} \\ &\quad - \Delta_y\{\Delta_y u + p_y \sigma^{-1}[(\mu_y - \mu_x)\, u + \rho q_x(\Delta_x f + \Delta_y g)]\} = 0. \qquad (3.4b) \end{aligned}$$

The values of u related by each of these equations are indicated in Fig. 4. We refer to (3.4) as the flux-eliminated form of (2.2). From its solution v and w may be calculated from (3.2).

When only u is prescribed on the boundary then (3.4) applies as indicated at all

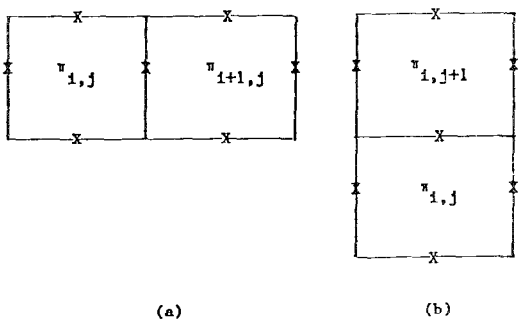

FIG. 4. Stencils for (3.4a), (3.4b).

interior points. When, more generally, v or w is prescribed at boundary points additional equations expressing these prescribed values are obtained from (3.2). Finally we call attention to the fact that the parameters h and v occur in (3.4) only in the combination $\rho = h/v$.

4. Limiting Forms of Flux-Eliminated Equations

As stated in the introduction we shall be interested in studying the solution $u(v, h)$ of (3.4) as $h \to 0$, $v(h) \to 0$. Depending on the function $v(h)$, as $h \to 0$, $\rho = h/v$ approaches 0, a constant, or ∞. In this section we shall describe some results of formally applying the limits $\rho \to 0, \infty$ in (3.4) using the asymptotic values for p, q given in (2.5). For our purpose it will be sufficient to examine only (3.4a).

Case 1. $\rho \to \infty$. When $\theta \simeq 0$ then $p \simeq 0$, $q \simeq 1/3$ and (3.4a) reduces to

$$(u_{i-1/2,j} + 10u_{i+1/2,j} + u_{i+3/2,j}) - 3(u_{i,j-1/2} + u_{i,j+1/2} + u_{i+1,j-1/2} + u_{i+1,j+1/2}) \simeq 0.$$

Case 2. $\rho \to \infty$. When $|\theta| \gg 1$ then $p \sim \operatorname{sgn}(\theta)$, $q \sim |\theta|^{-1}$ and so in this case different limiting forms arise depending on $\operatorname{sgn}(a)$, $\operatorname{sgn}(b)$ where $a = f_u$, $b = g_u$. We write

$$a_- \equiv a_{i,j}, \qquad a_+ \equiv a_{i+1,j},$$
$$b_- \equiv b_{i,j}, \qquad b_+ \equiv b_{i+1,j}.$$

(i) $a_\pm > 0$, $b_\pm > 0$. Equation (3.4a) reduces to

$$(b_- - a_-)\, u_{i-1/2,j} + (b_- + a_-)\, u_{i+1/2,j} - 2b_- u_{i,j-1/2} \simeq 0.$$

The relevant stencil is shown below with arrows indicating the direction of the inviscid characteristics. Note that the reduced equation uses only "upwind" infor-

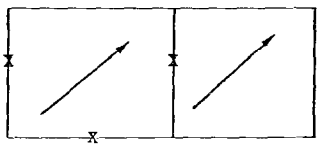

FIG. 5. Case (i).

mation to calculate $u_{i+1/2,j}$. In particular, if these two cells are the entire computatinal domain then the prescribed boundary values on the upwind side of $u_{i+1/2,j}$ solely determine its values. This corresponds to the analytic situation in which the inviscid weak solution requires boundary data only on the *inflow* part of the boundary at which characteristics enter the domain (see Fig. 5).

(ii) $a_+ < 0$, $a_- > 0$, $b_\pm > 0$ ($|b| \gg |a|$). Equation (3.4a) reduces to

$$a_- u_{i-1/2,j} + (a_- - a_+) u_{i+1/2,j} - a_+ u_{i+3/2,j} - 2a_- u_{i,j-1/2} + 2a_+ u_{i+1,j-1/2} \simeq 0.$$

Again $u_{i+1/2,j}$ is influenced only by upwind points as shown in Fig. 6.

(iii) $a_+ > 0$, $a_- < 0$, $b_\pm > 0$ ($|b| \gg |a|$). Here (see Fig. 7)

$$u_{i+1/2,j} - \tfrac{1}{2}(u_{i,j-1/2} + u_{i+1,j-1/2}) \simeq 0.$$

In interpreting these observations it must be remembered that corresponding equations arise from (3.4b). These examples provide useful insights into understanding the test problems considered in the next section. In these problems ρ varies from 0.3 to 40 with corresponding values of θ ranging from 0 to 40, so the actual finite difference equations can be very close to the different limiting forms in different parts of the domain.

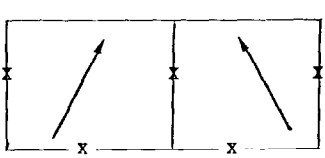

FIG. 6. Case (ii).

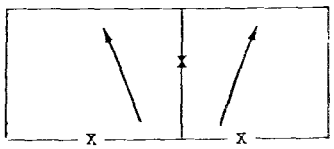

FIG. 7. Case (iii).

5. NUMERICAL EXAMPLES

We have indicated earlier that we may expect that the compact scheme (2.2) yields a solution $u(\nu, h)$ which converges to the solution $u(\nu)$ of (2.1) with an L_2 error of order h^2 (cf. Example 1). In this section we are primarily interested in studying the L_2 error E between $u(\nu, h)$ and the inviscid solution u^0 as $h \to 0$, $\nu \to 0$, by means of numerical experiments.

The first question which arises concerns the possibility of solving (3.4) for $u(\nu, h)$ when $\rho \to \infty$. Although several iterative methods were studied with, generally, successful results our report will concentrate on the use of the Gauss–Seidel method. One reason for our doing so stems from favorable results, as yet unpublished, by our colleague T. N. Phillips concerning the treatment of systems closely related to (3.4) by multigrid methods using Gauss–Seidel as the underlying iterative scheme.

A central question motivating this study is how effectively internal and external boundary layers arising from aproximating u^0 by $u(\nu, h)$ can be localized. A related question concerns the relative influence of the viscosity ν compared to inaccuracies arising from the fact that the scheme has truncation errors of order h^2. In order to help discuss this we introduce a parameter $\tau = h^2/\nu$ which together with $\rho = h/\nu$, will be used to study the solution as $h \to 0$, $\nu(h) \to 0$.

Another issue concerns insights into upwind difference schemes. As discussed earlier $|\theta| \ll 1$ leads to a diffusion-type limit of (3.4) while $|\theta| \gg 1$ leads to an inviscid upwind-type treatment. Both can occur if $\rho \gg 1$ and a (or b) passes through zero in some region. The functions p, q in (3.4) automatically handle this transition with a "viscous" treatment near $a \sim 0$ and an "almost-inviscid" treatment elsewhere.

The final matter concerns the question: under what limiting processes do nonconservative finite difference schemes yield the correct asymptotic inviscid result when $h \to 0$, $\nu(h) \to 0$?

The examples which follow address these questions. The first two examples graphically illustrate the behaviour of $u(\nu, h)$ in cases in which the inviscid limit u^0 is either linear or nonlinear. In the next five examples the L_2 error E between the solution $u(\nu, h)$ and the inviscid, analytic solution u^0 is computed for different values of ν, h, and the results are compared using simple heuristic analyses. The final example calculates the L_2 error for a problem using a nonconservative form of (3.4).

EXAMPLE 1. f and g are linear and are defined by

$$f = au, \qquad a = x - \tfrac{1}{2},$$
$$g = bu, \qquad b = 1 - y.$$

Note that $f_x + g_y = au_x + bu_y$ since $a_x + b_y = 0$. Hence the inviscid solution u^0 is constant along characteristics defined parametrically by

$$\frac{dx}{ds} = a, \qquad \frac{dy}{ds} = b, \qquad \text{i.e.,} \quad (1-y)(\tfrac{1}{2} - x) = \text{const.}$$

The domain considered is $0 \leqslant x \leqslant 1$, $0 \leqslant y \leqslant 1$ and so the only inflow boundary on which boundary data needs to be specified is on $y = 0$. The boundary values are chosen to be

$$u^0(x, 0) = \sin \pi(\tfrac{1}{2} - x),$$

so that the solution in the interior is

$$u^0(x, y) = \sin[\pi(1-y)(\tfrac{1}{2} - x)].$$

The boundary conditions for the finite difference problem are chosen to be

$$u(x, 1) = u^0(x, 1), \qquad u(0, y) = -1, \qquad u(1, y) = 1,$$

so that boundary layers arise at $x = 0, 1$.

Figure 8 shows contour plots of $u(\nu, h)$ for several different values of ν and h. Figures 8a–c illustrate ordinary convergence arising from a sequence in which ν is kept fixed and h is reduced by factor of 2 each time; little visual difference appears. Figures 8a–e are a sequence in which $\rho = h/\nu$ is kept fixed and h is reduced by factor of 2 each time; observe that the width of the boundary layers decreases. Finally, 8a, f, g illustrate a sequence in which h is kept fixed and ν is decreased by a factor of 4 each time. Note that the boundary layers at $x = 0, 1$ become smaller until they are confined to one interior cell.

EXAMPLE 2. This nonlinear example was suggested by our colleague E. Tadmor to test the ability of the scheme to converge to the correct "physical" inviscid solution for a problem with an infinite range of formal inviscid solutions. We consider

$$f = u^2, \qquad g = u^3.$$

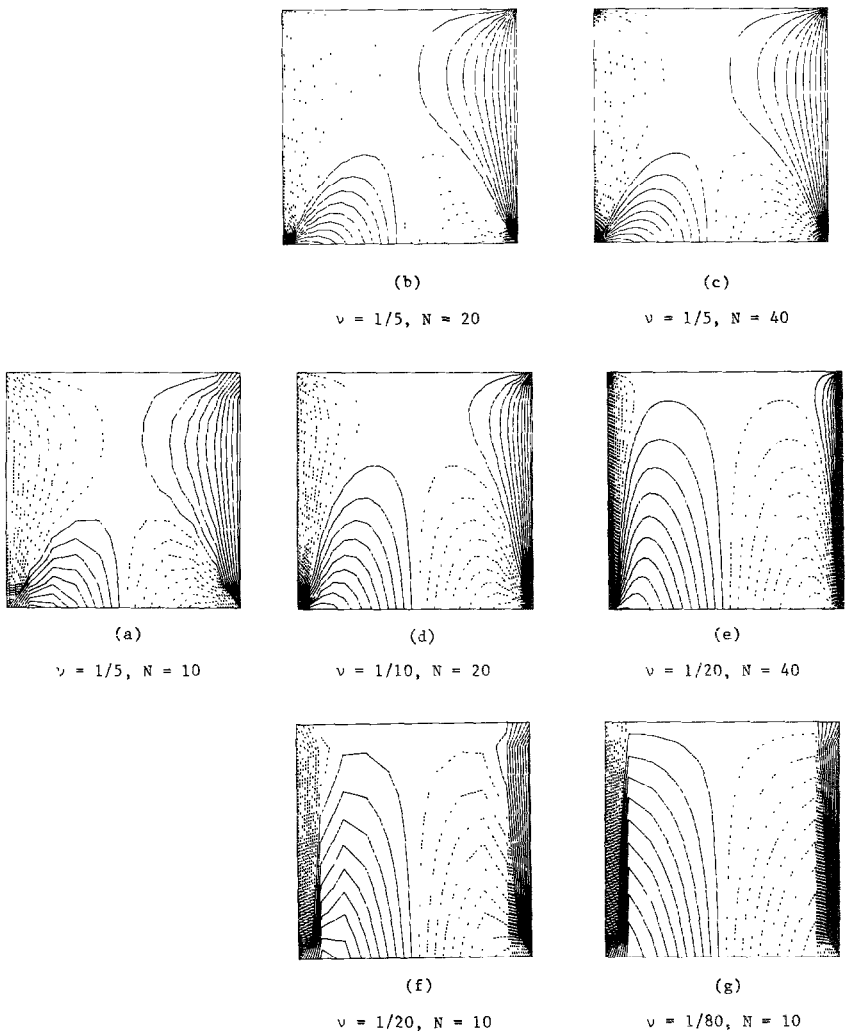

FIG. 8. Contour plots for Example 1; (a)–(c) illustrate ordinary convergence ($h \to 0$, $\nu = \text{const.}$); in (a), (d), (e) $\rho = \text{const.}$, $h \to 0$; in (a), (f), (g), $h = \text{const.}$, $\nu \to 0$. (In (f), (g) the boundary layer thickness is confined to one cell.).

The test case has an expansion fan attached to a shock

$$u^0(x,y)=\begin{cases}0.8, & \dfrac{x-0.3}{y}<\dfrac{1}{1.2},\\[2ex] \dfrac{2y}{3(x-0.3)}, & \dfrac{1}{1.2}<\dfrac{x-0.3}{y}<\dfrac{1}{0.6},\\[2ex] -0.2, & \dfrac{1}{0.6}<\dfrac{x-0.3}{y}.\end{cases}$$

The boundary conditions for the finite difference solution are $u(v,h)=u^0$ on all four sides so that the only sharp gradients occur at the shock.

Figure 9 shows contour plots of $u(v,h)$ for fixed ρ and decreasing h. In 9a the shock is indistinguishable from the expansion fan but in 9c the difference is obvious, and it is also clear that the numerical solution is converging to the "physical" inviscid solution.

EXAMPLE 3. This linear example uses the same definition of f and g as Example 1, and has the same inviscid solution u^0. However, this time the finite difference scheme has boundary conditions $u=u^0$ on all four sides of the square domain. Three cases were run, one with a 20×20 grid, and two with 80×80 grids keeping $\rho=h/v$ fixed in one case, and $\tau=h^2/v$ fixed in the other. Table I shows (i) the number of Gauss–Seidel iterations (starting from initial conditions $u=0$); (ii) the L_2 error E; (iii) E divided by the error E^* for the 20×20 grid, and (iv) the predicted ratio E/E^* based on the following simple analysis.

Let L_0 be the inviscid differential operator and $L(v,h)$ the viscous finite difference operator. Then

$$L_0u^0=0 \qquad \text{and} \qquad L(v,h)\,u(v,h)=0,$$

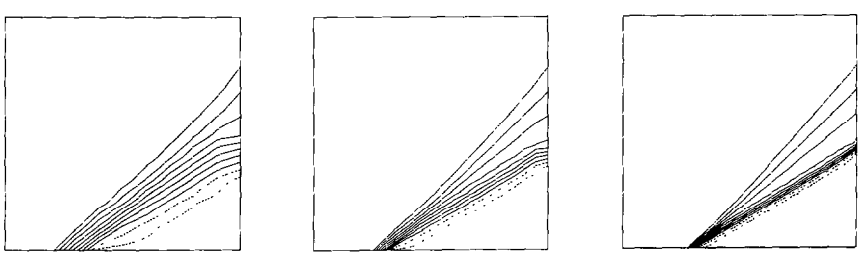

(a) (b) (c)

FIG. 9. Example 2, $f=u^2$, $g=u^3$; $\rho=$ const., $h\to 0$.

TABLE I

Results for Example 3

	$N = 20$	$N = 80$	
	$\rho = 10$ $\tau = 0.5$	$\rho = 10$ $\tau = 0.125$	$\rho = 40$ $\tau = 0.5$
No. of iterations	15	55	25
E	.334 (−2)	.821 (−3))	.216 (−3)
E/E^*	1	0.245	0.0647
Predicted ratio	1	0.25	0.0625

so

$$L(v, h)(u^0 - u(v, h)) = (L(v, h) - L_0)\, u^0 \sim h^2 \cdot \text{function}\left(\frac{h^2}{v}\right)$$

and $u^0 - u(v, h) = 0$ on the boundary; thus

$$\|u^0 - u(v, h)\|_{L_2} \sim h^2 e(\tau) \qquad \text{as} \quad h \to 0,$$

where $e(\tau)$ is some function of τ, the relative influence of truncation and viscosity.

EXAMPLE 4. This example has linear f, g

$$f = 0.5u, \qquad g = u$$

with discontinuous boundary data for which the inviscid solution u^0 is

$$u^0 = \begin{cases} 0.8, & x < 0.3 + 0.5y, \\ -0.4, & x > 0.3 + 0.5y. \end{cases}$$

The analysis for this case is not easy but leads to the result

$$E \sim h^{1/2} e(\tau),$$

where e is a function with asymptotic behaviour,

$$\tau \to 0, \qquad e \sim \tau^{-1/4} \Rightarrow E \sim v^{1/4}.$$

Thus when τ is small the error E is due not to the second-order truncation but rather to the viscous smearing of the contact discontinuity (see Table II).

EXAMPLE 5. This example is a two-dimensional version of Burgers' equation with a shock:

$$f = 0.5u^2, \qquad g = 0.4u$$

TABLE II

Results for Example 4

	$N=20$	$N=80$	
	$\rho=0$ $\tau=0.5$	$\rho=10$ $\tau=0.125$	$\rho=40$ $\tau=0.5$
No. of iterations	10	15	15
E	.144	.0969	.0901
E/E^*	1	0.673	0.625
Predicted ratio	1	0.707	0.5

and the inviscid solution u^0 is

$$u^0 = \begin{cases} 0.8, & x < 0.3 + 0.5y, \\ -0.4, & x > 0.3 + 0.5y. \end{cases}$$

In the finite difference solution the shock becomes an internal boundary layer with width of order v. If $\rho = h/v$ is kept fixed as $h \to 0$ this shock layer is spread over the same number of cells and hence

$$E \sim h^{1/2} e(\rho).$$

As $\rho \to 0$, $e \sim \rho^{-1/2} \Rightarrow E \sim v^{1/2}$ and so when ρ is small the error is due solely to a physically well-resolved shock (see Table III).

EXAMPLE 6. This example is exactly the same as Example 1 except for different values of h and v. The analysis cannot be expressed in one simple equation. If $\rho \to 0$ and $h \to 0$ then $E \sim v^{1/2}$ since the boundary layer has thickness of order v and so it is well resolved. If ρ is kept fixed the boundary layer spans a fixed number of cells and so $E \sim h^{1/2}$. If τ is kept fixed it has an $O(h)$ effect on just the interior points adjacent to the boundary and so $E \sim h^{3/2}$ (see Table IV).

TABLE III

Results for Example 5

	$N=20$	$N=80$	
	$\rho=10$ $\tau=0.5$	$\rho=10$ $\tau=0.125$	$\rho=40$ $\tau=0.5$
No. of iterations	35	85	85
E	.102	.050	.048
E/E^*	1	.49	.47
Predicted ratio	1	.5	.5

TABLE IV

Results for Example 6

	$N = 20$	$N = 80$	
	$\rho = 10$ $\tau = 0.5$	$\rho = 10$ $\tau = 0.125$	$\rho = 40$ $\tau = 0.5$
No. of iterations	15	55	25
E	.448 (−1)	.254 (−1)	.51 (−2)
E/E^*	1	0.567	0.114
Predicted ratio	1	0.5	0.125

EXAMPLE 7. This example is the same of Example 3 except that the boundary condition at $y = 1$ is $u(x, 1) = 1$ which produces a boundary layer at $y = 1$. This boundary layer is different from the ones in Example 6. In Example 6 the boundaries were *outflow* boundaries, i.e., the inviscid characteristics were pointing outwards across the boundary. In this example the characteristics are tangential to the boundary at $y = 1$, similar to a stagnation point flow in fluid dynamics.

The physical boundary has thickness of order $\nu^{1/2}$ so if τ is kept fixed as $h \to 0$ it spans a fixed number of cells and $E \sim h^{1/2}$. Hence

$$E \sim h^{1/2} e(\tau)$$

and as $\tau \to 0$, $e \sim \tau^{-1/4} \Rightarrow E \sim \nu^{1/4}$ (see Table V).

Table VI summarizes the results of Examples 3.7.

EXAMPLE 8. This example studies a nonconservative form of the compact equations obtained by replacing the term $\delta_x f + \delta_y g$ in (2.2a) by $\bar{a}\delta_x u + \bar{b}\delta_y u$ where $\bar{a}$, $\bar{b}$ are average values of f_u and g_u in the cell. The test case is

$$f = u^4, \qquad g = 0.4u$$

TABLE V

Results for Example 7

	$N = 20$	$N = 80$	
	$\rho = 10$ $\tau = 0.5$	$\rho = 10$ $\tau = 0.125$	$\rho = 40$ $\tau = 0.5$
No. of iterations	20	60	25
E	.149	.107	.074
E/E^*	1	0.718	0.498
Predicted ratio	1	0.707	0.5

TABLE VI

Summary of Asymptotic Behaviour of E

E	$\nu = \text{const}$	$\rho = \text{const.}$	$\tau = \text{const.}$
Smooth u^0	ν	h	h^2
Linear, discontinuous u^0	$\nu^{1/4}$	$h^{1/4}$	$h^{1/2}$
Nonlinear, discontinuous u^0	$\nu^{1/2}$	$h^{1/2}$	$h^{1/2}$
Smooth u^0, "wrong" outflow boundary conditions	$\nu^{1/2}$	$h^{1/2}$	$h^{3/2}$
Smooth u^0, "wrong" tangent boundary conditions	$\nu^{1/4}$	$h^{1/4}$	$h^{1/2}$

with an inviscid solution

$$u^0 = \begin{cases} 0.8, & x < 0.3 + 0.5y, \\ -0.4, & x > 0.3 + 0.5y. \end{cases}$$

The error analysis shows that E has two components, E_1 due to shock smearing, and E_2 due to an incorrect shock angle.

$$\begin{aligned} E_1 &\sim (\text{shock width})^{1/2} \\ &\sim \nu^{1/2} = h^{1/2}\rho^{-1/2} \\ E_3 &\sim (\text{conservation loss per unit shock length})^{1/2} \\ &\sim [(\#\text{ cells across shock}) \times (\#\text{ cells along shock}) \\ &\qquad \times (\text{truncation error per cell})]^{1/2} \\ &\sim \left[\frac{\nu}{h} \times \frac{1}{h} \times \frac{h^3}{\nu^2}\right]^{1/2} \\ &\sim \rho^{1/2}. \end{aligned}$$

The two error components have the same order of magnitude when $\rho \sim h^{1/2}$. If $\rho \ll h^{1/2}$, E_1 dominates and, if $\rho \gg h^{1/2}$, E_2 dominates. Hence,

$$\begin{aligned} E &\sim \nu^{1/2}, \qquad \rho \ll h^{1/2}, \\ &\sim \rho^{1/2}, \qquad \rho \gg h^{1/2}, \end{aligned}$$

and at each fixed h, E is minimized by choosing $\rho \sim h^{1/2}$, and $E_{\min} \sim h^{1/4}$.

The top of Table VII shows results from several experiments and the bottom portion has the corresponding values of $E_{\min}/h^{1/4}$ and $\rho_{\min}/h^{1/2}$ which, according to the analysis, should be constants.

TABLE VII

E / ρ	N = 20	N = 80
0.31	.267	.162
0.62	.220	.121
1.25	.168	.133
2.5	.228	.266
5	.376	.393
$E_{\min}/h^{1.4}$	.355	.362
$\rho_{\min}/h^{1.2}$	.18	.18

6. Concluding Remarks

The experiments reported in the previous section suggest that the compact scheme (2.2) provides an effective means of approximating both $u(v)$ and u^0 and that the relationship between these solutions which is suggested by singular perturbation arguments is maintained, as indicated by Fig. 1, by the finite difference scheme as well. A fact of potential practical importance is that boundary layers can be confined to a single computational cell. This feature is a relevant factor as well in selecting the conservative form of (2.2) instead of the nonconservative form.

Finally, the fact that the flux-eliminated equations (3.4) can be treated by a Gauss–Seidel iterative method indicates that a wide variety of more rapid iterative methods can also be employed. In contrast, the use of time-stepping methods to obtain $u(v)$ or u^0 can be seen to result in a more slowly convergent Jacobi-type iteration scheme.

References

1. F. A. Howes, Perturbed boundary value problems whose reduced solutions are nonsmooth, *Indiana Univ. Math. J.* **30** (1981), 267–280.
2. F. A. Howes, Perturbed elliptic problems with essential nonlinearities, *Comm. Partial Differential Equations* **8** (1983), 847–874.
3. J. Kevorkian and J. D. Cole, "Perturbation Methods in Applied Mathematics," Springer, New York, 1981.
4. S. Osher, The numerical solution of singular perturbation problems and hyperbolic systems of conservation laws, *in* "Analytical and Numerical Approaches to Asymptotic Problems in Analysis," pp. 179–204, North-Holland, New York, 1981.
5. R. B. Philips and M. E. Rose, Compact finite difference schemes for mixed initial-boundary value problems, *SIAM J. Numer. Anal.* **19** (4) (1982), 698–720.
6. T. N. Phillips and M. E. Rose, "A finite difference scheme for a class of first order elliptic partial differential equations." *Comput. Math. Appl.*, to appear.
7. M. E. Rose, Compact finite difference schemes for the Euler and Navier–Stokes equations, *J. Comput. Phys.* **49** (1983), 420–442.